A Computational Study of the Biomechanical Response of the Human Lower Extremity Subjected to High Rate Vertical Accelerative Loading

Zachary S. Hostetler, Jazmine Aira, Joel D. Stitzel, F. Scott Gayzik

Abstract Vertical loading in the underbody blast (UBB) condition generates high accelerative loading at the contact points between the occupant and vehicle, particularly the lower extremity. The objective of this study is to use the Global Human Body Models Consortium (GHBMC) average male lower extremity to quantify loads experienced in representative UBB conditions. A secondary aim is to evaluate the stability and robustness of the model in these conditions. A design of experiments (DOE) was conducted using the GHBMC M50-O v. 4.5 leg (proximal tibia through foot). The DOE consisted of forty-nine simulations in which the time-to-peak (TTP), acceleration, jerk, and pulse duration were varied, matching previously published data of UBB events. Peak kinematics were extracted from virtual load cells at the knee, tibia, and calcaneus. Fracture risk for the lower extremity was assessed using published risk curves for the UBB environment. All 49 simulations normal terminated. Accelerations ranged from 45 G's to 1665 G's. The peak knee, tibia, and calcaneus forces were 11.3, 13.6 and 14.9 kN respectively. Twenty-six of the 49 simulations resulted in a fracture risk greater than 0.5, thus the majority of the simulated trials indicated the presence of injury. The GHBMC M50-O lower extremity model was stable and robust in the simulated UBB environments.

Keywords GHBMC, human body model, lower extremity, under-body blast.

I. INTRODUCTION

Underbody blast (UBB) events have become a leading cause of warfighter casualties in modern conflicts [1, 2]. The lower extremity is highly susceptible to injury due to the nature of the loading [3]. Injury to the lower extremity is caused by the high rate vertical loading to the lower limb, frequently resulting in bone fracture [4]. Recent studies have used various human surrogates including the Warrior Injury Assessment Manikin (WIAMan) anthropomorphic test device (ATD), the Hybrid-III ATD, or post-mortem human subjects (PMHSs) in the study of UBB [5-8].

The UBB environment has distinct characteristics from the automotive environment that forms the foundation of many injury biomechanics studies involving human surrogates. Previous studies have highlighted the differences in the blast itself; the peak acceleration in the UBB environment is 5 to 10 times larger than automotive impacts, and the duration of the pulse is 3 to 5 times shorter [7]. To better understand the loading parameters, this group conducted a computational study using a model of the Hybrid-III ATD in a drop tower test rig. The goal was to examine the effects of the peak acceleration, pulse duration, change in velocity (delta-v) and the rate of acceleration onset. Pulse durations for the study ranged from 2.5 ms to 60 ms and peak accelerations ranged from 10 G's to 1200 G's. Other research has been focused on the impact and injury response of PMHSs compared to the Hybrid III ATD. A previous study found that damage to the calcaneus occurred 2 ms after the floor began moving.

Z.S. Hostetler is a PhD student in Biomedical Engineering, J. Aira is a Research Engineer in the Dept. of Biomedical Engineering, J.D. Stitzel is a Professor of Biomedical Engineering and F.S. Gayzik (sgayzik@wakehealth.edu, +1 336-716-6643) is an Associate Professor of Biomedical Engineering at Wake Forest University School of Medicine, USA

Furthermore there were limitations with the Hybrid III ATD in that it could not assume the posture of the PMHS in the rig, and its overall response was much stiffer [8]. In recent years, the development of the WIAMan ATD has been a major contributor to the foundational biomechanics in the UBB environment.

The WIAMan ATD has been used in UBB testing conditions to evaluate its biofidelity [9].

Human body models (HBMs) are another tool that can be leveraged in the study of UBB. HBMs can be tested in a range of environments and speeds for less cost and in less time than their physical surrogate counterparts. They are designed for omnidirectional impact, and developed directly from human anatomy. They are not limited by the potential tradeoff between biofidelity and the requirement to be ruggedised enough to withstand physical testing. Lastly, these models can be positioned into different postures and rigs, and tested at the subsystem level like ATDs and PMHS. While HBMs can be programmed to directly calculate tissue level failure through element elimination, they can also be used to calculate injury risk directly from human injury risk curves without the need for injury assessment reference curves commonly employed in ATDs, e.g., IARCs. The Global Human Body Models Consortium (GHBMC) M50-O average male seated occupant is a widely used and validated HBM [10-12]. Its geometry is based on images collected *ad hoc* for the purposes of model development and represents a 50th percentile average male [13]. The GHBMC has been tested previously in the UBB environment with a focus on the pelvic response [14]. The lower extremity of the GHBMC has been validated in various loading conditions, including axial loading [15, 16]. While these studies were developed for the automotive environment, there were a number of cases that tested loading in the axial direction as occurs in UBB. These include, the tibial shaft in lateral and medial bending, the lower leg in combined compression and bending as well as the foot in combined loading and axial impact [23,16]. The GHBMC model version 3.4 was tested in this environment previously [17]. The mesh updates and material updates for the flesh have been added to the version 4.5 of the GHBMC model used in the current study.

Building on the research with ATD's and PMHSs, there is a need to further explore the UBB environment using computational human models. The objective of this study was to use the GHBMC average male lower extremity to quantify the resulting gross loads experienced in representative UBB conditions. A secondary aim is to evaluate the stability and robustness of the model in these conditions.

II. METHODS

Modelling Overview

To simulate a laboratory UBB environment, the GHBMC M50-O v. 4.5 lower extremity (proximal tibia to foot) was disarticulated from the whole body. The leg was virtually fitted within a simulation boundary condition mimicking a previously published rig known as the Vertically Accelerated Load Transfer System (VALTS) [6, 18]. The rig consists of a cantilevered arm mimicking the femur and knee and a plate that impacts the foot vertically. The physical system that the model is based on has been used in previous studies of UBB loading [6, 19-21]. Personal protective equipment (PPE) in the form of a boot was fitted onto the foot of the GHBMC. The sponsor of this research furnished the boot model (U.S. Army Research Lab). Boot fitment was accomplished by artificially decreasing the size of the foot to fit within the native boot and then allowing the human foot model to linearly increase to its nominal size. The process achieved a smooth fit between the human model's leg and foot and the surrounding boot. The ankle is natively at a 90-degree angle from the leg and was remained at that angle following the boot donning process.

Leg placement and axis orientation in the virtual rig followed previous experimental work with PMHS test conditions [22]. The depression on the tibial plateau was aligned in the centre of a modelled poly-methyl-methacrylate (PMMA) block. The tibia was embedded into this block, similar to a potting procedure, to a depth of 30 mm. Coordinate axis were defined by a landmark on the superior-most aspect of the tibia, medial malleolus, and the anterior malleoli [22]. The total weight of the lower extremity with the PPE boot was 4.77 kg. The mass of the plate from the test rig striking the boot was 3.1 kg. For all simulations, explicit fracture in all bones (tibia, fibula, calcaneus, and talus) was disabled for stability purposes.

Simulation Pulses

A design of experiments (DOE) was conducted for a range of underbody blast (UBB) conditions to study the sensitivity of the GHBMC lower extremity in a range of inputs. The sample space was derived from previously-published data on the UBB environment [5, 7, 8, 23-25]. The DOE varied the following parameters: pulse duration (ms), time to peak acceleration (ms), peak acceleration (G's) and jerk (G's/ms). The sample space was derived by fitting a function (Equation 1) to the peak accelerations reported at different pulse durations in [7]. In this study, simulations were run using a human surrogate (Hybrid III) at the full body level. We have adopted these input condition in a more controlled environment using the GHBMC lower extremity. Here *a(t)* = acceleration (G's) and *t* is the pulse duration (milliseconds).

$$a(t) = 2381.46 * e^{-0.354t} + 216.02 \quad (1)$$

Equation 1 represents 100% of the peak acceleration from [7]. For the present study, the function in Equation 1 was sampled at 20, 40, 60, 80, 100, 110 and 120 % of this value to test the robustness of the model. The function was evaluated at 2, 4, 6, 8, 10, 12, and 15 millisecond pulse durations. To vary the jerk, each simulation's time to peak acceleration was randomly chosen to be between ¼ and ½ of the pulse duration (where acceleration was positive). This sampling led to 49 unique simulation pulses over the range of the sample space (dots in Figure 1).

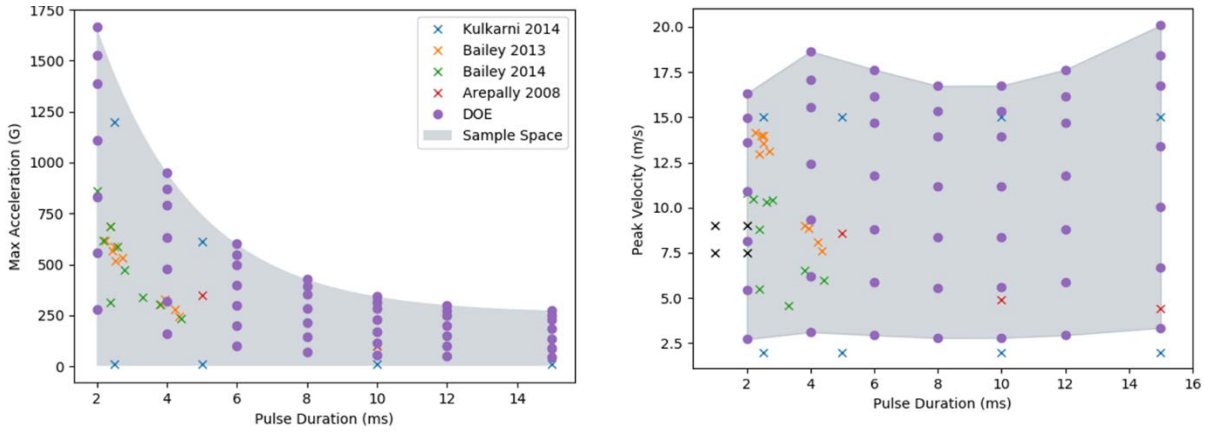

Fig. 1. Pulse duration vs. peak acceleration (left) and velocity (right) showing the DOE sample space. The peak respective value of each simulation, as well as previous literature studies are shown. Each dot shows a sample within the DOE space while the x's represent tests in previously-published studies.

The acceleration profiles for the simulations were integrated and prescribed as a velocity vs. time motion to the floor plate in the simulated rig. An example acceleration profile showing the four varied parameters and resulting velocity input prescribed to the floor is shown in Figure 2.

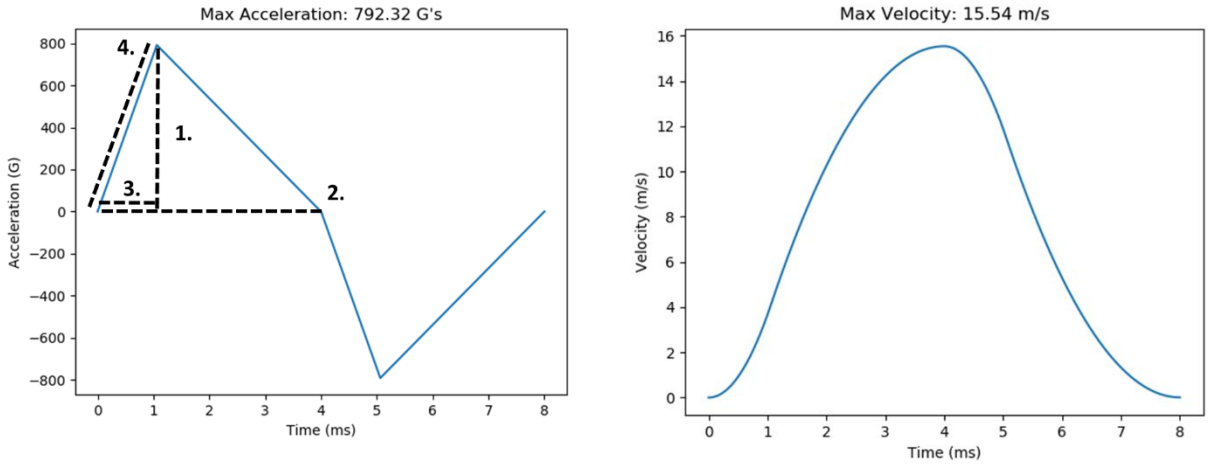

Fig. 2. Input simulation parameters for acceleration profiles (left) with varying input parameters. 1, peak acceleration, 2, pulse duration (ms), 3, time to peak acceleration, and 4, jerk (G/ms). The resulting velocity curve is shown on the right.

Instrumentation

The GHBMC M50-O lower leg was instrumented with virtual load cells to output data at similar locations as were reported in published studies [22, 26-28]. Force data were extracted from these virtual load cells located at the knee, proximal, middle and distal tibia, as well as the calcaneus. Peak forces, leg compression, energy absorbed by the leg, and lower leg fracture risk [29] were calculated for all 49 simulations. Figure 3 shows the instrumented GHBMC lower extremity in the test setup.

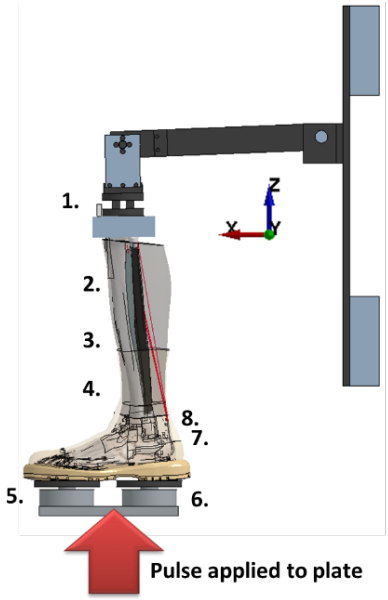

Figure 3. The GHBMC M50-O 4.5 lower extremity in the test rig with implemented instrumentation to align with previous UBB studies. 1, knee load cell (LC) and accelerometer. 2, Proximal tibia LC and strain gage. 3, Middle tibia LC. 4, Distal tibia LC. 5, Toe plate LC. 6, Heel Plate LC. 7, Transverse calcaneus LC and accelerometer. 8, Medial calcaneus strain gage.

To calculate the energy absorbed by the leg, a force transducer was instrumented at the bottom of the foot to directly measure the plantar force at the point of contact between the foot and sole of the boot. Two nodes were identified, one at the top of the tibia and one on the bottom of the foot flesh. From these two nodes, vertical change in length, e.g., displacement, of the leg in the z-direction was

calculated. The resulting force-displacement curve was integrated to obtain a measure of energy absorbed by the leg (J). Using published risk curves for lower leg fracture risk contour plots of injury risk (from 0-5 %, 5-50 %, and 50-100%) as a function of pulse duration and velocity where generated. These graphs serve as an objective way to evaluate injury risk by pulse duration and peak velocity. Contour plots of energy and distal tibia force were also generated.

The material models are documented in the GHBMC M50-O v 4.5 however, they are briefly summarized here. Cortical bone is modeled with shell elements for the calcaneus and talus as well as for the epiphyses of the tibia and fibula. The shaft of the long bones are modeled with solid elements. Cortical bone is modeled as a plastic kinematic material and the solid cortical bone includes strain rate dependency (ρ = 2 g/cm^3, E = 17.5 GPa, ν = 0.3, σ_y = 125 to 165 MPa, E_t = 0.7 to 1 GPa). The cancellous bones are modeled with solid elements as a plastic kinematic material (ρ = 1.1 g/cm^3, E = 0.45 GPa, ν = 0.3, σ_y = 0.005 GPa). The flesh uses a simplified hyper elastic rubber model (rho =1.06 g/cm^3, K = 2 GPa) and material uniaxial behavior data taken from [30].

III. **RESULTS**

All 49 simulations normal terminated showing robustness and stability of the GHBMC model in the UBB environment. Pulse durations varied from a minimum of 4 milliseconds to 30 milliseconds. Acceleration at the loading plate ranged from 45 G's to 1665 G's with TTP values of 15 ms and 2 ms respectively. The jerk ranged from 8.22 G/ms to 2162.62 G/ms. All simulations followed the general trend of attenuation from distal to proximal locations on the leg. The average force across all simulations moving up the leg was: 6.25, 7.06, 6.97, 6.27 and 5.31 kN in the calcaneus, distal tibia, middle tibia, proximal tibia and knee respectively. This trend can be seen in Figure 4 where larger negative forces indicate greater compressive forces. The magnitude of the force is reduced as it traverses the leg. The calcaneus peak is less due to multiple load paths from that point to the leg. The plantar force is the highest measured force as expected because it is measured directly at the bottom of the foot flesh.

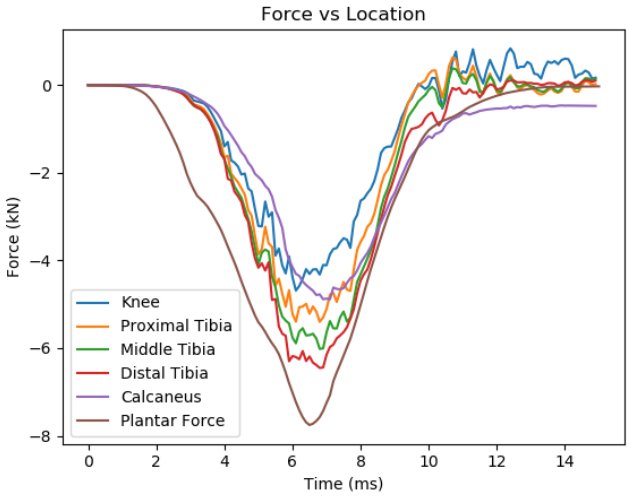

Fig. 4. Force attenuation trend seen in the DOE where force dissipates as it moves up the leg.

Peak acceleration across all simulations was highest in the calcaneus at 1316 G's and lowest in the knee at 767 G's. Max displacement between the knee and the calcaneus were similar at 462.6 mm and 466.7 mm whereas tibia displacement was lower at 363.6 mm. The range of energy absorbed directly by the leg ranged from 2.3 J to 515.3 J. The average lower leg fracture risk was 52%. Inputs from each simulation can be found in Table A1 and simulation outputs can be found in Table A2 of the appendix. A contour plot of lower leg (tibia, fibula, calcaneus and talus) fracture risk as a function of pulse duration and peak velocity are shown in Figure 5. This plot interpolates between the tests in the DOE. There is a

high chance of fracture for the short pulse durations with high peak velocity (14+ m/s) and risk chance also increases as pulse duration increases at moderate velocity (12-14 m/s).

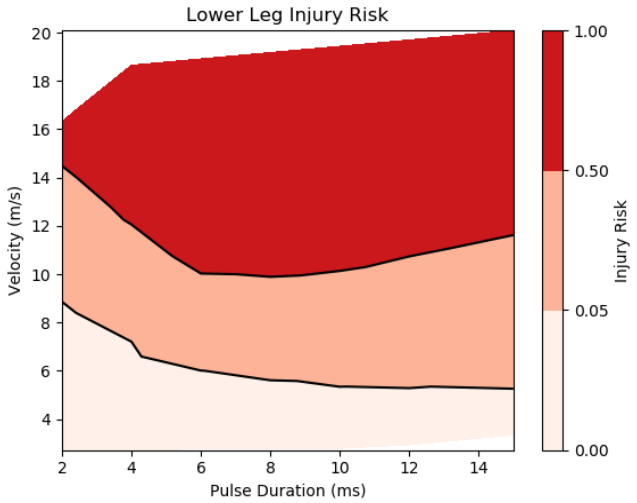

Fig. 5. Lower leg fracture risk shown as a function of pulse duration (ms) and peak velocity (m/s).

Figure 6 details the range of force observed in the tibia as well as the energy absorbed by the leg in all 49 simulations. For very short pulse durations with high velocity, or longer pulse durations with moderate velocity, the force of the tibia reached up to 15 kN in our simulations and energy absorbed reached 600 J. Table 1 details the range of input parameters that were used in the DOE and expand upon previously published UBB values.

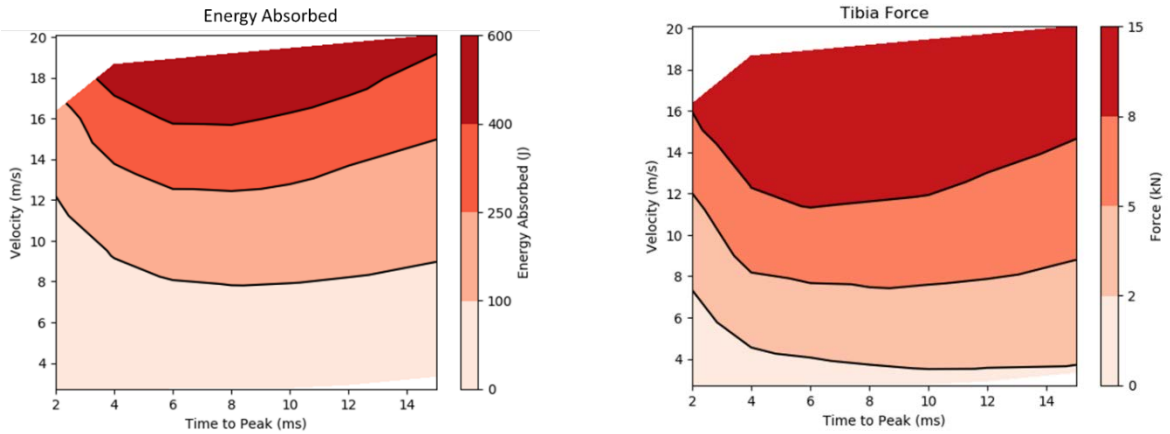

Fig. 6. Range of energy absorbed by the leg in the DOE (left) and range of tibia force experienced by the leg in the DOE (right)

TABLE I
RANGE OF INPUT PARAMETERS FOR THE DOE CONDUCTED WITH THE GHBMC M50-O LOWER LEG.

	Pulse Duration (ms)	Acceleration (G's)	Time to Peak (ms)	Jerk (ms/G)	Velocity (m/s)
Min	2	45	0.53	8.2	2.7
Max	15	1665	6.46	2162.6	20.1

IV. DISCUSSION

The sample space of the DOE was representative of previous values reported for UBB. The range of peak acceleration was extended outside of previously studied values to test the stability and robustness of the GHBMC model. The model showed stability in all 49 simulations conducted. The peak accelerations reported in Table 1 are greater than what has previously been reported and this is likely due to testing outside of the range of previous accelerations. Floor velocities reported from the DOE exceed the 10 to 12 m/s range reported by [24] and the 15 m/s reported by [7]. While no explicit valuation in this condition was included as part of this work (given previous validation efforts and the goal of the study), leg compression compares well to values reported by [22].

The risk curve chosen for this study was developed by [29] and the predictor variable of peak plantar force is intended to be independent of varying boundary conditions conducted from previous studies [22, 26, 27, 31]. The selected risk curve was developed with both booted and non-booted data, but a single risk curve was published. We selected the plantar surface of the foot to evaluate all data. We believe this is a reasonable assumption since recent studies have not included PPE as a covariate in the risk curve [25,28]. Fracture risk was evaluated using curves from [26] however, they resulted in very low fracture risk. This is likely because the input variable is peak knee force and these forces were slightly lower than reported by [26]. This can be contributed to difference of the boundary condition of the plate mass striking the leg (6.2 kg vs 3.1 kg).

The lower leg injury risk curve and the contour plots of different levels of injury risk (0-5, 5-50, and 50-100%) provide potentially valuable information for injury risk given pulse duration and peak velocity. The data could be of use in the design of PPE equipment (boots) as well as guide for requirements in vehicle hull design. The injury risk for the lower leg followed a *U-shaped* curve in the contour plots. This resulted in injury risk increasing again at longer pulse durations but lower peak velocity. Although the energy absorbed in the longer pulses was lower, the foot was in contact with the foot plate for longer compared to the shorter duration pulses. Therefore, the foot reached greater velocity the longer it was in contact with the foot plate in these cases.

Previous studies detailed the development of a foot and ankle model for UBB [32] but did not include any anatomy beyond the ankle, nor a range of loading scenarios. The work presented in this study expands beyond the foot and ankle into the tibia and knee and models a more complete lower extremity. Previous work in UBB has been done with ATDs or PMHSs [5-7, 24] but to the authors' knowledge this is among the first to utilise human models in a DOE for the UBB environment. The energy absorbed by the leg can be used as a reference value to potentially translate to ATD results where stiffness mismatches make matched pair testing challenging. Thus, the data here could be helpful in the generation of Injury Assessment Reference Values (IARVs) for ATDs in the UBB condition.

For all simulations, fracture of bones (tibia, fibula, calcaneus, and talus) was turned off. This may be viewed as a limitation since fracture was likely to have occurred in the severe accelerative loadings and this would in turn affect peak force, moment and acceleration data. However, such fracture dynamics are difficult to predict, and from a injury mitigation standpoint it is most valuable to understand the point of injury and attempt to design below it. Furthermore, there were no pre-strains in the ligaments or Achilles tendons. The foot (with boot) was gravity settled onto the plate in pre-simulation positioning, but pre-strains are typically not added in PMHS UBB trials. The loading direction generally places the leg in compression and the main load path is through the cartilage that surrounds the calcaneus, talus and distal tibia/fibula upward, limiting the effect of the ligaments. Based on these two factors, omitting pre-strain was deemed a reasonable simplification. Lastly, for the energy absorbed and compression of the leg, the values were calculated in the z-direction and did not account for displacement in other directions. However, since the test setup is primarily loaded in the vertical (Z) direction other displacements would be negligible.

V. CONCLUSIONS

The GHBMC M50-O lower extremity model was simulated in 49 UBB-like events that were designed based on a range of loading scenarios reported in the literature. The majority of the simulated trials indicated the presence of injury. The model was found to be robust and stable in this environment and was used to produce contour plots showing risk of injury of the lowerI leg along with other biomechanical parameters. This simulated approach can provide insight and guidance on the lower extremity injury risk from severe vertical loading.

VI. ACKNOWLEDGEMENT

Funding for this work was provided by U.S. Army Med R & D Command, under BAA W911NF-17-S-0003, *Exploring Physics-based Finite Element Analysis of Service Members Subjected to Extreme Environments*. The authors acknowledge the contributions and support of Dr. Michael Kleinberger, Mr. Randolph Coates, and Dr. Kathryn Loftis of the U.S. Army Futures Command. F.S. Gayzik and J.D. Stitzel are members of Elemance, LLC, which provide academic and commercial licenses for GHBMC-owned models.

VII. REFERENCES

1. Bird, S. and C. Fairweather, *Recent military fatalities in Afghanistan (and Iraq) by cause and nationality.* MRC Biostatistics Unit, UK, 2010.
2. Wilson, C. *Improvised explosive devices (IEDs) in Iraq and Afghanistan: effects and countermeasures*. 2007. LIBRARY OF CONGRESS WASHINGTON DC CONGRESSIONAL RESEARCH SERVICE.
3. Ramasamy, A., et al., *Injuries from roadside improvised explosive devices.* Journal of Trauma and Acute Care Surgery, 2008. **65**(4): p. 910-914.
4. Ramasamy, A., et al., *In-vehicle extremity injuries from improvised explosive devices: current and future foci.* Philosophical Transactions of the Royal Society B: Biological Sciences, 2011. **366**(1562): p. 160-170.
5. Bailey, A., et al. *Comparison of Hybrid-III and PMHS response to simulated underbody blast loading conditions*. in *Proceedings of IRCOBI Conference*. 2013.
6. Baker, W.A., et al., *Mechanical characterization and finite element implementation of the soft materials used in a novel anthropometric test device for simulating underbody blast loading.* Journal of the mechanical behavior of biomedical materials, 2017. **74**: p. 358-364.
7. Kulkarni, K.B., J. Ramalingam, and R. Thyagarajan, *Assessment of the accuracy of certain reduced order models used in the prediction of occupant injury during under-body blast events.* SAE International journal of transportation safety, 2014. **2**(2): p. 307-319.
8. Danelson, K.A., et al., *Comparison of ATD to PMHS response in the under-body blast environment*. 2015, SAE Technical Paper.
9. Pietsch, H.A., et al., *Evaluation of WIAMan technology demonstrator biofidelity relative to sub-injurious PMHS response in simulated under-body blast events*. 2016, SAE Technical Paper.
10. Vavalle, N.A., *Validation of the Global Human Body Models Consortium Mid-Sized Male Model in Lateral Impacts and Sled Tests*. 2012, Wake Forest University.
11. Hayes, A.R., et al., *Validation of simulated chestband data in frontal and lateral loading using a human body finite element model.* Traffic injury prevention, 2014. **15**(2): p. 181-186.
12. Gayzik, F.S., et al. *Development of a full human body finite element model for blunt injury prediction utilizing a multi-modality medical imaging protocol*. in *12th International LS-DYNA User Conference, Dearborn, MI*. 2012.
13. Gayzik, F., et al., *Development of a full body CAD dataset for computational modeling: a multi-modality approach.* Annals of biomedical engineering, 2011. **39**(10): p. 2568.

14. Weaver, C.M., A.C. Merkle, and J.D. Stitzel, *Pelvic Response of a Total Human Body Finite Element (FE) Model During Simulated Under Body Blast (UBB) Impacts.*
15. Untaroiu, C.D., N. Yue, and J. Shin, *A finite element model of the lower limb for simulating automotive impacts.* Annals of biomedical engineering, 2013. **41**(3): p. 513-526.
16. Yue, N., J. Shin, and C.D. Untaroiu, *Development and validation of an occupant lower limb finite element model*. 2011, SAE Technical Paper.
17. Gabler, L.F., M.B. Panzer, and R.S. Salzar. *High-rate mechanical properties of human heel pad for simulation of a blast loading condition*. in *Proceedings of the IRCOBI Conference*. 2014.
18. Baker, W.A., M. Chowdhury, and C.D. Untaroiu, *A finite element model of an anthropomorphic test device lower limb to assess risk of injuries during vertical accelerative loading.* Journal of biomechanics, 2018. **81**: p. 104-112.
19. Merkle, A.V., L; Ott, K; Dooley, C; Carneal, C. *APL Status Update*. in *Medical Research Meeting* 2012. Ft. Rucker.
20. Ott, K., et al. *Initial characterization of the human response to vertical accelerative loading*. in *Seventh World Congress of Biomechanics*. 2014.
21. Ott, K.L., Q; Andrist, J; Arminger, R; Carneal, C; Merkle, A. *Replicating Live-Fire Test Conditions in a Laboratory Environment*. in *Proc. Military Health Systems Research Symp*. 2016.
22. Pintar, F.A., et al., *Biomechanical response of military booted and unbooted foot-ankle-tibia from vertical loading*. 2016, SAE Technical Paper.
23. Arepally, S., et al., *Application of mathematical modeling in potentially survivable blast threats in military vehicles*. 2008, ARMY TANK-AUTOMOTIVE RESEARCH AND DEVELOPMENT CENTER WARREN MI.
24. Bailey, A.M., et al., *Post mortem human surrogate injury response of the pelvis and lower extremities to simulated underbody blast.* Annals of biomedical engineering, 2015. **43**(8): p. 1907-1917.
25. Kulkarni, K.B., J. Ramalingam, and R. Thyagarajan, *Evaluating the effectiveness of various blast loading descriptors as occupant injury predictors for underbody blast events*. 2013, ESI US INC TROY MI.
26. Chirvi, S., et al., *Human foot-ankle injuries and associated risk curves from under body blast loading conditions*. 2017, SAE Technical Paper.
27. Gallenberger, K., N. Yoganandan, and F. Pintar, *Biomechanics of foot/ankle trauma with variable energy impacts.* Annals of advances in automotive medicine, 2013. **57**: p. 123.
28. Yoganandan, N., et al., *Foot–ankle fractures and injury probability curves from post-mortem human surrogate tests.* Annals of biomedical engineering, 2016. **44**(10): p. 2937-2947.
29. Bailey, A.M., et al., *Survival model for foot and leg high rate axial impact injury data.* Traffic injury prevention, 2015. **16**(sup2): p. S96-S102.
30. Yamada, H. and F.G. Evans, *Strength of biological materials.* 1970.
31. Funk, J.R., et al., *The axial injury tolerance of the human foot/ankle complex and the effect of Achilles tension.* Journal of biomechanical engineering, 2002. **124**(6): p. 750-757.
32. Grigoriadis, G., et al. *A finite element model of the foot and ankle for prediction of injury in under-body blast*. 2016. IRCOBI.

VI. APPENDIX

TABLE A1
SIMULATION INPUT SUMMARY FOR THE 49 TRIALS OF THE DESIGN OF EXPERIMENTS STUDY

Sim Index	TTP (ms)	Pulse Dur. (ms)	Acc. (G)	Vel. (m/s)	Jerk (G/ms)	Sim Index	TTP (ms)	Pulse Dur. (ms)	Acc (G)	Vel (m/s)	Jerk (G/ms)
1	0.53	2	277.5	2.7	523.7	26	2.27	8	355.4	13.9	156.6
2	0.9	2	554.8	5.4	616.7	27	3.4	8	391.0	15.3	115.0
3	0.73	2	832.4	8.2	1140.6	28	3.56	8	426.5	16.7	119.8
4	0.79	2	1109.8	10.9	1405.2	29	4.64	10	56.9	2.8	12.3
5	0.88	2	1387.1	13.6	1576.9	30	4.72	10	113.8	5.6	24.1
6	0.9	2	1525.8	15.0	1696.1	31	4.36	10	170.7	8.4	39.2
7	0.77	2	1664.7	16.3	2162.6	32	4.33	10	227.7	11.2	52.6
8	1.85	4	158.4	3.1	85.7	33	4.46	10	284.6	14.0	63.8
9	1.05	4	316.9	6.2	301.9	34	3.36	10	313.1	15.4	93.2
10	1.98	4	475.2	9.3	240.1	35	4.17	10	341.5	16.7	81.9
11	1.62	4	633.8	12.4	391.3	36	4.16	12	50.0	2.9	12.0
12	1.93	4	792.1	15.5	410.6	37	3.93	12	99.9	5.9	25.4
13	1.84	4	871.3	17.1	473.8	38	4.88	12	149.9	8.8	30.7
14	1.63	4	950.6	18.7	583.4	39	3.2	12	199.8	11.8	62.4
15	2.64	6	99.9	2.9	37.9	40	3.29	12	249.8	14.7	75.9
16	2.37	6	199.8	5.9	84.3	41	5.97	12	274.6	16.2	46.0
17	1.6	6	299.7	8.8	187.4	42	5.63	12	299.7	17.6	53.2
18	2.54	6	399.6	11.8	157.4	43	5.54	15	45.5	3.3	8.2
19	1.66	6	499.6	14.7	301.0	44	4.69	15	91.1	6.7	19.4
20	1.84	6	549.6	16.2	298.7	45	4.39	15	136.6	10.0	31.1
21	2.53	6	599.5	17.6	237.0	46	3.94	15	182.1	13.4	46.2
22	2.26	8	71.1	2.8	31.5	47	5.9	15	227.6	16.7	38.6
23	3.7	8	142.2	5.6	38.4	48	4.36	15	250.4	18.4	57.4
24	2.34	8	213.3	8.4	91.2	49	6.46	15	273.2	20.1	42.3
25	2.11	8	284.3	11.2	134.8						

TABLE AII

SELECT SIMULATION OUTPUT MEASURES FOR THE 49 DOE TRIALS.

MEASURES WITH AN (*) ARE INCLUDED IN THE BODY OF THE PAPER AS CONTOUR PLOTS.

Sim Index	Middle Tibia Force (kN) *	Transverse Calcaneus Force (kN)	Knee LC Force (kN)	Lower Leg Fracture Risk *	Leg Compression (mm)	Energy *
1	0.39	0.13	0.26	0.00	4.22	2.34
2	1.16	0.42	0.86	0.00	7.99	12.17
3	2.37	1.01	1.88	0.02	11.87	34.07
4	4.16	1.87	3.26	0.12	16.24	73.09
5	6.19	3.25	4.60	0.39	20.36	129.30
6	7.45	4.19	5.67	0.56	22.15	162.54
7	8.21	5.00	6.12	0.72	23.81	198.41
8	1.00	0.40	0.73	0.00	8.69	7.25
9	3.16	1.58	2.54	0.00	16.10	39.70
10	6.08	4.23	4.96	0.15	22.91	103.87
11	8.10	6.98	6.26	0.55	29.16	195.16
12	10.60	9.83	8.18	0.93	35.48	322.23
13	12.36	11.18	9.46	0.99	38.52	398.38
14	14.09	12.76	10.72	1.00	41.61	487.14
15	1.12	0.57	0.93	0.00	11.07	10.03
16	3.42	2.25	2.74	0.04	19.02	49.47
17	6.02	4.89	4.69	0.33	25.90	117.41
18	8.35	7.90	6.57	0.75	32.41	216.10
19	11.44	10.43	8.56	0.98	38.89	343.66
20	13.31	12.79	9.95	1.00	41.99	422.71
21	14.60	14.87	11.30	1.00	45.04	515.27
22	1.23	0.71	1.04	0.00	12.15	11.17
23	3.55	2.33	2.74	0.05	19.98	50.21
24	5.69	4.69	4.24	0.30	26.53	112.39
25	7.62	7.49	5.59	0.67	32.68	197.55
26	9.93	10.03	7.64	0.98	38.54	311.79
27	11.83	11.63	9.05	1.00	41.28	380.33
28	13.16	13.58	10.18	1.00	44.41	461.05
29	1.43	0.78	1.15	0.00	13.00	12.50
30	3.67	2.46	2.57	0.05	20.68	51.39
31	5.52	4.69	4.09	0.28	26.85	109.65
32	7.39	7.20	5.32	0.63	32.79	189.56
33	9.62	9.39	7.38	0.97	38.55	294.43
34	11.07	10.73	8.34	1.00	40.80	348.15
35	11.70	12.73	9.35	1.00	44.00	426.34

36	1.53	0.88	1.18	0.00	13.81	14.16
37	3.72	2.58	2.59	0.06	21.37	53.85
38	5.61	4.79	3.95	0.28	27.53	112.18
39	7.07	6.97	5.01	0.62	32.98	185.16
40	9.25	8.96	7.07	0.96	38.56	284.30
41	10.61	11.28	8.51	1.00	41.73	355.13
42	11.88	12.78	9.00	1.00	44.46	424.14
43	1.78	1.03	1.43	0.00	14.91	17.19
44	3.85	2.90	2.68	0.08	22.48	60.02
45	5.69	5.06	3.90	0.32	28.46	119.13
46	7.17	7.18	5.05	0.70	34.19	197.16
47	9.41	9.50	7.42	0.99	40.42	309.70
48	10.03	11.04	8.15	1.00	42.43	363.62
49	11.58	12.87	8.86	1.00	46.11	445.96